Nuclear Inst. and Methods in Physics Research, A 1034 (2022) 166824

Contents lists available at ScienceDirect

Nuclear Inst. and Methods in Physics Research, A

journal homepage: www.elsevier.com/locate/nima

Investigation on the performance of a thick ceramic gas electron multiplier

Zhimeng Hu [a,b,c], Andrea Muraro [d], Giuseppe Gorini [b,c,d], Oisin McCormack [b], Enrico Perelli Cippo [d], Marco Tardocchi [d], Zhijia Sun [e,f,*,1], Xiaojuan Zhou [e,f], Jianrong Zhou [e,f,*,1], Yuguang Xie [f], Yuanbo Chen [e,f], Hui Zhang [h,1,**], Tieshuan Fan [g], Gabriele Croci [b,c,d,1,***]

[a] Department of Nuclear Science and Technology, Nanjing University of Aeronautics and Astronautics, 211106 Nanjing, China
[b] Dipartimento di Fisica, Università degli Studi di Milano-Bicocca, 20126 Milano, Italy
[c] INFN Sezione di Milano-Bicocca, 20126 Milano, Italy
[d] Institute for Plasma Science and Technology, National Research Council, 20125 Milan, Italy
[e] Spallation Neutron Source Science Center, 523803 Dongguan, China
[f] Institute of High Energy Physics, Chinese Academy of Sciences, 100049 Beijing, China
[g] National Institute of Metrology, 100029 Beijing, China
[h] School of Physics and State Key Laboratory of Nuclear Physics and Technology, Peking University, 100871 Beijing, China

ARTICLE INFO

Keywords:
Ceramic gas electron multiplier
Effective gain
Resolution

ABSTRACT

We report the performance of a THick Gas Electron Multiplier (THGEM) fabricated by drilling holes in a gold-clad ceramic substrate using the standard PCB (Printed Circuit Board) technology and etching rims. The THGEM has a total thickness of 200 μm with a hole diameter and rim size of 200 μm and 80 μm, respectively. In order to carry out a performance study, a detector was assembled by putting the THGEM inside a versatile chamber and irradiating it with a ^{55}Fe X-ray source (5.9 keV). An Ar/CO_2 gas mixture was flushed inside the chamber at a pressure of about 1 atm, with volume ratios varying between 70/30 and 90/10. Pulse height spectra of the detector were recorded by a multichannel analyzer to investigate the gain and energy resolution at different drift and induction electric fields. The variations in the gain and energy resolution were also interpreted using simulations. The gain and resolution data of the THGEM were compared with those of a standard GEM which was measured using the same experimental setup.

1. Introduction

The gas electron multiplier (GEM) [1], one of the most popular Micro-Pattern Gas Detectors, has excellent particle detection capabilities, e.g., high count rate (~MHz/mm^2) [2], good spatial resolution (~50 μm) [3], and good timing resolution (~5 ns) [3]. When combined with the appropriate electronics, GEMs have various applications in high energy physics, nuclear physics, dosimetry domains, neutron science, and plasma diagnostics [1–6]. In particular, neutron applications profit from the low background sensitivity of GEM based detectors [7], a technology originally proposed by F. Sauli at CERN in 1996 [8]. A high-density array of holes inside a thin metal-clad insulation foil can provide strong dipole electric fields, after supplying high voltage across the foil, to multiply the electrons released by ionizations in the drift region above a GEM. The standard GEM is the most widely utilized version of the technology, which has bi-conical shape holes with 50-70 μm diameter. Its hole pitch and total thickness are 140 μm and 60 μm, respectively [3].

THick GEMs (THGEMs) are more robust and more easily manufactured with respect to the standard GEMs [9–11], with the THGEMs having >5 times larger dimensions, e.g., in foil thickness and hole diameter. They can be produced by drilling holes in an insulator substrate using standard PCB technology and rim-etching. The rim structure enables a THGEM to reach higher gains and be more immune to discharges. THGEMs can measure various particles like the standard GEM and find many applications, for instance in the COMPASS RICH (Ring-Imaging Cherenkov Counter) system at CERN [12–14], in Digital Hadronic Calorimeters at the International Linear Collider [15], and in developing readouts of double phase detectors [16,17]. They have also found wide application in neutron and medical physics [18–25].

A new THGEM was developed using the standard PCB (Printed Circuit Board) technology at the Chinese Spallation Neutron Source [19]. This THGEM has a total thickness of 200 μm with a hole diameter and rim size of 200 μm and 80 μm, respectively. The substrate of this THGEM is made from ceramics which is a hydrogen free material. Therefore,

* Corresponding authors at: Spallation Neutron Source Science Center, 523803 Dongguan, China.
** Corresponding author at: National Institute of Metrology, 100029 Beijing, China.
*** Corresponding author at: Dipartimento di Fisica, Università degli Studi di Milano-Bicocca, 20126 Milano, Italy.
E-mail addresses: sunzj@ihep.ac.cn (Z. Sun), zhoujr@ihep.ac.cn (J. Zhou), zhanghui@nim.ac.cn (H. Zhang), gabriele.croci@unimib.it (G. Croci).
[1] The orders of the corresponding authors: Gabriele Croci, Zhijia Sun, Jianrong Zhou, Hui Zhang.

https://doi.org/10.1016/j.nima.2022.166824
Received 20 September 2021; Received in revised form 7 April 2022; Accepted 28 April 2022
Available online 6 May 2022

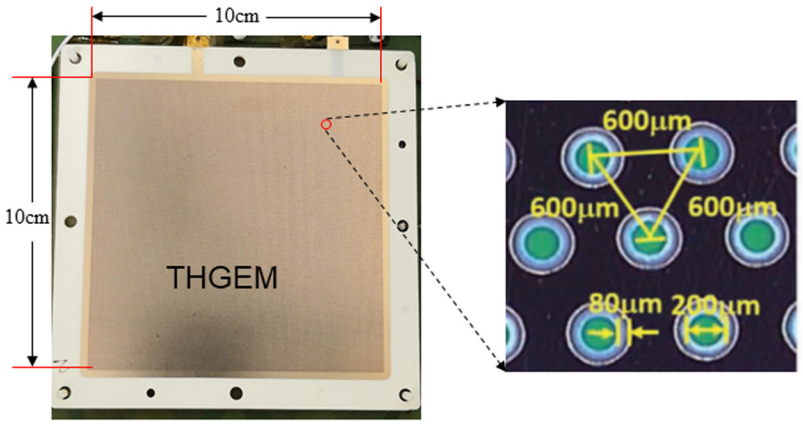

Fig. 1. A picture of the THGEM and a schematic of the THGEM holes.

compared to other THGEMs, for example based on FR-4 substrates, it has lower neutron scattering, making it a better choice to use in thermal neutron detectors. The out-gassing of the THGEM is lower, as requested, and it thus provides a solution to develop sealed detectors.

In this study, we carry out a comprehensive investigation on the gain and energy resolution performance of a single ceramic THGEM based detector under an ^{55}Fe X-ray source (5.9 keV). The content of the paper is as follows. A detector was built by putting a THGEM foil in a versatile chamber. The relationships between effective gains and high voltages across the THGEM (V_{THGEM}) were measured to choose the appropriate V_{THGEM}. The effective gain and energy resolution variations with the drift electric field (E_d) and with the induction electric field (E_{in}) were then measured while the THGEM worked at different volume ratios of Ar/CO_2 gas mixtures. The variations with E_d for the gain and energy resolution were also explained by comparing with simulations. Replacing the THGEM with a standard GEM and using the same experimental setup, the gain and energy resolution of a standard GEM were determined and compared with those obtained by the THGEM. The gain and resolution stability of the THGEM and standard GEM are also tested.

2. Materials and methods

2.1. The THGEM description

The THGEM (10 × 10 cm^2 active area, as shown in Fig. 1) used in this study is composed of a substrate with metal electrodes on both sides and a total thickness of 200 μm. The cylindrical holes are in a hexagonal array with a diameter, pitch, and rim size of 200 μm, 600 μm, and 80 μm, respectively. Each electrode is 15 μm thick and realized by depositing copper and then gold on substrate surfaces. The 170 μm thick substrate is a composite by mixing pure ceramics with 10 wt% glass fiber [19]. Its main components, including oxygen, silicon, and aluminum, are 48.5 wt%, 34.3 wt% and 8 wt%, respectively. The THGEM was realized by using standard PCB technology.

2.2. Experimental setup

Fig. 2 shows the layout of the detector which consists of a cathode and an anode with a single THGEM in between, and is placed inside a versatile chamber. The cathode is a thin copper foil deposited on a thin Kapton plate, and the anode is a copper plane. The thickness of the drift and induction regions is 1.8 mm and 3.2 mm, respectively. The distance between the Kapton window and the cathode is about 3 mm. Inside the chamber, the total flow of Ar/CO_2 gas with a pressure of about 1 atm is 5 L/h which is controlled by two gas flow meters provided by Bronkhorst [25]. X-rays emitted by a ^{55}Fe source (5.9 keV) are collimated by a cylindrical hole and enter the detector through the thin

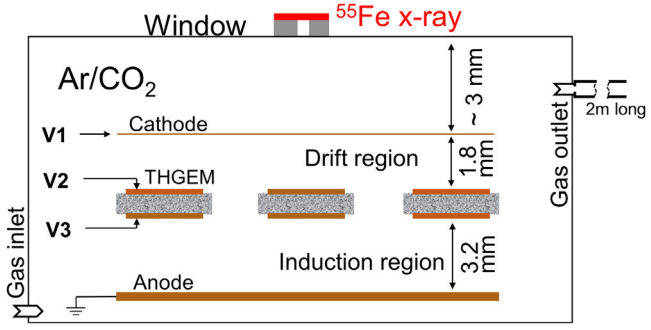

Fig. 2. Schematics of the test setup.

window. The activity of the source is 370 kBq as of March 2016 and the experiment was carried out in November 2019. The high voltages at the cathode, anode, and the THGEM electrodes are powered by two high voltage supplies (CAEN N1471 A). Output signals from the detector are fed into a preamplifier (ORTEC 142), followed by a shaping amplifier (ORTEC 570) with a shaping time of 0.5μs, and finally analyzed by a multichannel analyzer (ORTEC EASY-MCA) to give the pulse height spectrum (PHS).

3. Results

3.1. Effective gain variation with V_{GEM}

The effective gain variation as a function of V_{THGEM} was measured at E_d = 1.4 kV/cm and E_{in} = 1.6 kV/cm (see Fig. 3). The volume ratios of Ar/CO_2 gas used in the measurement are 70/30, 80/20, 85/15, and 90/10. A standard GEM is also measured using the same experimental setup after replacing the THGEM with a gold-clad standard GEM in the chamber. Effective gain data of the THGEM and the standard GEM are obtained from the full energy peak positions of the PHS. The gain data of a standard GEM [26] are used to derive the relationship between the channel number of an MCA and the absolute gain values. The GEM has a maximum gain comparable with the work in [26] after considering the influence of different E_{in} values on the gains. The full energy peak (5.9 keV) and the argon escape peak (2.9 keV) are clearly visible. The data at the full peak of the PHS are fitted with a Gaussian function to derive the peak position and full-width-at-half-maximum (FWHM). The detailed fitting process can be found in Ref. [27]. In Fig. 3, the y-axis is presented in logarithmic scale, so the linear relationship reveals the exponential dependence of effective gains of the THGEM on V_{THGEM}. This behavior is similar with that of the standard GEM. It can be seen that the maximum achieved gains of the THGEM are ~2 times higher

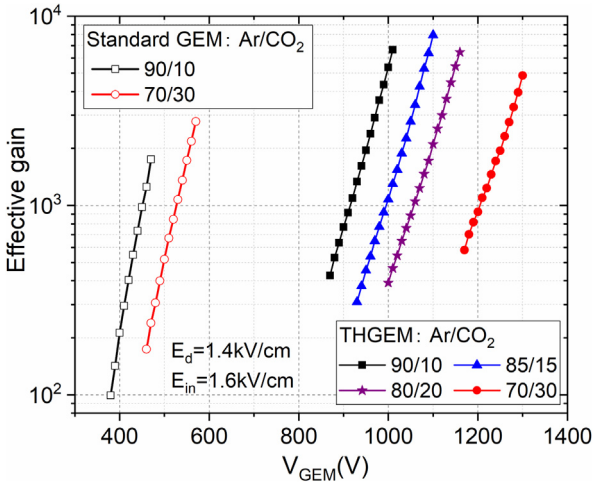

Fig. 3. Effective gain of the THGEM (and standard GEM) as a function of V_{THGEM} (and V_{GEM}) at several Ar/CO_2 gas mixtures.

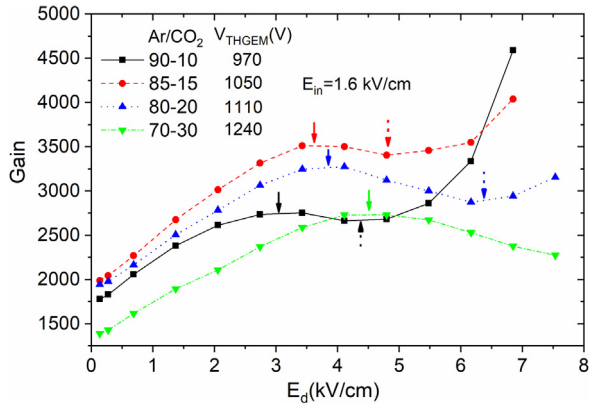

Fig. 4. Effective gain variation with E_d for the THGEM. The solid vertical line arrows represent the E_d where the gain reaches its maximum. The dotted vertical line arrows represent the E_d where the second increase on the gain starts. Source: These data are obtained from Ref. [27].

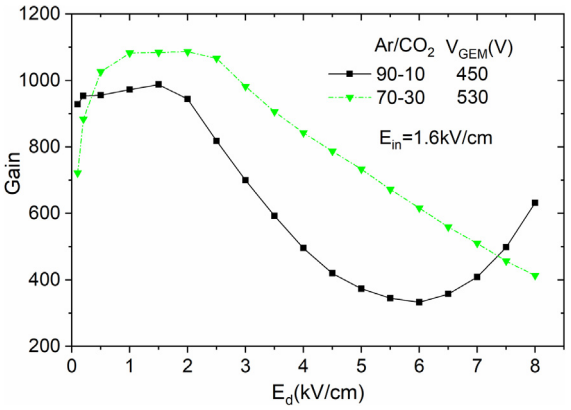

Fig. 5. Effective gain variation with E_d for the standard GEM. The error bar of each data is smaller than the marker size. Source: These data are obtained from Ref. [27].

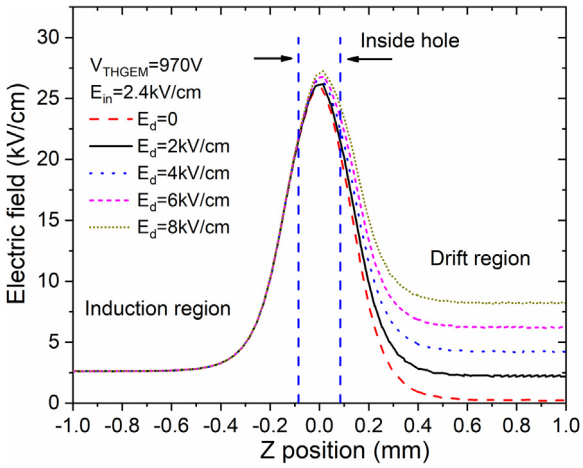

Fig. 6. Ansys-calculated results of electric field strength along the hole axis of the THGEM. z axis is along the hole axis, and the plane of $z = 0$ is at the middle-plane of the THGEM foil.

than the standard GEM. Suitable V_{THGEM}(and V_{GEM}) values, about 40 V lower than the limits to avoid discharges, were then chosen to carry out the measurement of effective gain and energy resolution at different E_d and E_{in}.

3.2. Effective gain variation with E_d

3.2.1. Experimental results

The effective gain variations with E_d in a range up to about 8 kV/cm were measured when the volume proportions of Ar/CO_2 gas changed between 90/10 and 70/30. The experimental results are depicted in Fig. 4. These gains increase by more than 60% when incrementing E_d and reaches a peak indicated by solid vertical line arrows in Fig. 4. This continuously increasing phenomenon is also found in other THGEMs with rims [10]. Above peak positions, the gains have a slight decrease, and then increase again with increasing E_d. For larger Ar/CO_2 proportions, the peak positions and the E_d values where the second increase of gain (indicated by dotted vertical line arrows in Fig. 4) starts to move towards lower E_d values.

As shown in Fig. 5, the effective gain variation as a function of E_d for the standard GEM using the same experimental setup as the THGEM was also measured, except that the thickness of the drift region is 3 mm. For $Ar/CO_2 = 90/10$, below peak positions the gain increases by about 10% to reach the maximum, and then it decreases rapidly. When E_d is higher than ~5.5 kV/cm, the gain increases again. For $Ar/CO_2 = 70/30$, a sharp increase of the effective gains below E_d ~1 kV/cm can be explained by the electron recombination in gas. This is different from the gain variation for $Ar/CO_2 = 90/10$ where a sharp increase below E_d ~0.2 kV/cm seems to show the presence of the electron recombination. For $Ar/CO_2 = 70/30$ at high E_d, the second increase of effective gains does not behave the same way as when Ar/CO_2 is 90/10 due to the lower Townsend coefficients in Ar/CO_2 (70/30) gas.

3.2.2. Explanation of the effective gain variation with E_d

Effective gain variations with E_d for the THGEM and standard GEM have been investigated in detail [27] by also taking into account the charging up effect. The experimental variations in the E_d ranging up to 8 kV/cm were quantitatively predicted by calculations via investigating the respective influence of increasing E_d on the electron collection efficiency (ECE) of holes and the gain augmentation. Below the peak positions, the increase of effective gain is due to the growing extension of the electric fields out of the holes when increasing E_d, which can be reflected by the distribution of the electric field strength along the hole axis at different E_d, as shown in Fig. 6. Effective gain variation with E_d is determined by the change of ECE and the gain enhancement due to electric field extension out of the holes. The peak positions measured are consistent with the upper limit of the corresponding ECE plateau in the low E_d range. The second increase on gain is ascribed to the growing extension of the electric fields out of the holes when increasing E_d, even though the ECE is simultaneously decreasing.

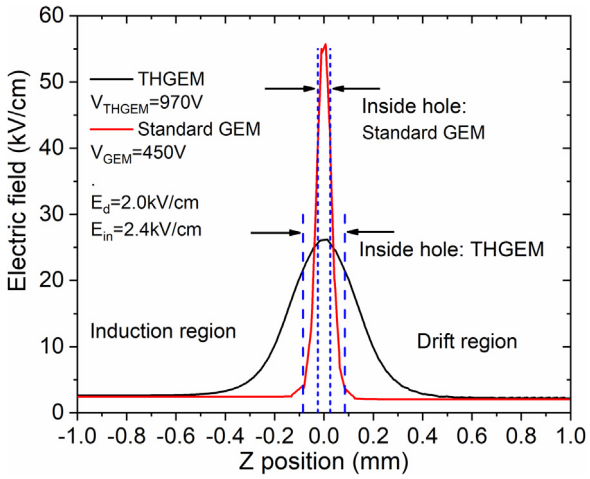

Fig. 7. Ansys-calculated results of electric field strength along the hole axis for the THGEM with V_{THGEM} = 970 V, and for the standard GEM with V_{GEM} = 450 V.

The THGEM has larger holes than the standard GEM, therefore the THGEM has a wider ECE plateau in the low E_d range, and above the upper limit of the plateau the ECE also decreases slower than for the standard GEM. In addition, the gain enhancement of the THGEM is stronger resulting from the larger extension of the electric fields out of the holes when increasing E_d. Fig. 7 shows an example of the comparison of electric field distributions along the hole axis between the THGEM and standard GEM. These results can reveal the differences in effective gain variation with E_d between the THGEM and standard GEM. For example, when increasing E_d the standard GEM has less increase of gain below peak positions, and the gain decreases faster above peak positions.

3.3. Resolution variation with E_d

3.3.1. Experimental results

Fig. 8 depicts measured resolutions of the THGEM varying with E_d. The corresponding effective gain data of the THGEM are shown in Fig. 4. The resolution data represent the FWHM value divided by the peak position at the full energy peak of a pulse height spectrum. The resolution is higher in the low E_d range below peak positions, then it becomes worse with increasing E_d. At high E_d values (above the dotted vertical lines in Fig. 4), the increase of effective gain does not help improve the resolution of the THGEM. This phenomenon is contrary with that found in the standard GEM, as shown in Figs. 8(a) and 9(a). We will explain this phenomenon in Section 3.3.2. In Fig. 8, even though we got the resolution data in the E_d range up to 8 kV/cm, in high E_d the resolution is so bad that it is hard to evaluate the uncertainties. In addition, a THGEM does not operate well in such a bad resolution mode. We thus do not provide here the resolution data much larger than 0.5, which is also done in Fig. 9 for the standard GEM.

In Figs. 8 and 9, the resolution at higher E_{in} is a little better because higher E_{in} helps the anode to collect electrons coming from the holes. Moreover, as seen in Fig. 8, the resolutions of the THGEM at two different E_{in} values have similar values in the E_d range of the measurement.

3.3.2. Explanation of the resolution variation with E_d

The pulse amplitude of a GEM is proportional to the number of electrons $\boldsymbol{Q}$ collected in the anode. The energy resolution is determined by the fluctuation of $\boldsymbol{Q}$ which consists of three parts: the variances of primary ionization, of ECE, and of the single electron multiplication factor [28]. For a GEM, the averaged Q can be expressed as

$$\overline{Q} = \overline{N} \cdot \overline{\varepsilon} \cdot \overline{G} = \overline{N} \cdot \overline{\varepsilon} \cdot \overline{G_t}.\overline{G_b}, \quad (1)$$

where N is the number of primary electrons produced in the drift region due to X-rays, the ε is the probability that the primary electrons (~230) are able to drift into holes, G is the single electron multiplication factor in the holes. Varying E_d almost does not change the electric field beneath the middle plane of the THGEM and the standard GEM [26,27]. In order to simplify the subsequent calculation of Q variations, we further divide G into two parts, G_t and G_b, respectively representing the single electron multiplication factor above and beneath the middle plane of GEM holes.

Using the formula (1), the relative standard variation of Q can be written as:

$$\left(\frac{\sigma_Q}{\overline{Q}}\right)^2 = \left(\frac{\sigma_N}{\overline{N}}\right)^2 + \left(\frac{\sigma_\varepsilon}{\overline{\varepsilon}}\right)^2 + \frac{1}{\overline{N}\cdot\overline{\varepsilon}}\left(\frac{\sigma_{G_t}}{\overline{G_t}}\right)^2 + \frac{1}{\overline{N}\cdot\overline{\varepsilon}\cdot\overline{G_t}}\left(\frac{\sigma_{G_b}}{\overline{G_b}}\right)^2, \quad (2)$$

Then the energy resolution of GEMs, defined as the ratio of the FWHM in the full energy peak to the peak position, can be derived as $2.235\cdot\frac{\sigma_Q}{\overline{Q}}$.

For the first component in formula (2), the variation of N can be expressed as $\left(\frac{\sigma_N}{\overline{N}}\right)^2 = F/\overline{N}$, where F is the Fano factor [29], $\overline{N} \approx 230$ is the average number of primary electron-ion pairs produced in Ar/CO_2 gas due to the ^{55}Fe X-ray source. In the Ar/CO_2 gas, an F value of 0.2 is employed. We can then derive $\frac{\sigma_N}{\overline{N}} = 3\%$. The contributions of this and all other components to the resolution are shown in Figs. 10 and 11.

The electric field in the drift and top half hole regions varies with E_d, and will modify ε and G_t [26]. We calculated the 2nd and 3rd components using the Garfield++ code. For each E_d, 500 runs were carried out. A hole is designed to collimate the primary X rays entering the drift region and the incident 5.9 keV photons in Ar/CO_2 gas have an absorption length of 2 cm, far larger than the drift region thickness (1.8 mm). Therefore, the distribution of primary electrons produced in the drift region is almost uniform. For each run, 230 electrons are produced uniformly in the drift region, and then drift towards the holes. The resulting contribution from the 2nd component, $2.235\cdot\sqrt{\left(\frac{\sigma_\varepsilon}{\overline{\varepsilon}}\right)^2}$, in different E_d are shown in Fig. 10 for the THGEM, and in Fig. 11 for the standard GEM working in Ar/CO_2 gas. The submission of the 2nd and 3rd resolution components, $2.235\cdot\sqrt{\left(\frac{\sigma_\varepsilon}{\overline{\varepsilon}}\right)^2 + \frac{1}{\overline{N}\cdot\overline{\varepsilon}}\left(\frac{\sigma_{G_t}}{\overline{G_t}}\right)^2}$, is calculated by further taking into account the avalanche process above the middle plane of the holes. The 3rd resolution component, $2.235\cdot\sqrt{\frac{1}{\overline{N}\cdot\overline{\varepsilon}}\left(\frac{\sigma_{G_t}}{\overline{G_t}}\right)^2}$, is thus obtained by quadratically subtracting the 2nd component from the aforementioned submission term. These resolution components are depicted in Figs. 10 and 11.

For the fourth component, the multiplication distribution of single electrons $\frac{\sigma_{G_b}}{\overline{G_b}}$ is calculated using the Garfield++ code as well. In this calculation, the electrons start from the middle plane of the holes for the THGEM and the standard GEM. The number distribution of electrons along the radius in the middle plane is used for initiating the simulation of single electron gain distribution beneath the middle plane of the two GEMs, shown in Fig. 12. The simulated data are fitted with the Polya function, which is usually used to describe the gain distribution of single electrons in gas. The Polya function can be expressed as:

$$f\left(G_b, \overline{G}_b, \theta\right) \propto \left[(\theta+1)\cdot\frac{G_b}{\overline{G}_b}\right]^\theta \cdot \exp[-(\theta+1)\cdot\frac{G_b}{\overline{G}_b}], \quad (3)$$

where θ is the parameter able to determine the variation of Polya distribution via $\left(\frac{G_b}{\overline{G}_b}\right)^2 = \frac{1}{1+\theta}$. The θ for the THGEM and the standard GEM are determined to be respectively 0.27 and 0.48. Despite a large difference for the θ value between the THGEM and the standard GEM, the contribution to the gain variation of the two GEMs, $\left(\frac{G_b}{\overline{G}_b}\right)^2$, is close, respectively from 0.74 to 0.79 and 0.68, which are close to the data in [28]. It is also found that the θ parameter does not depend on the E_d

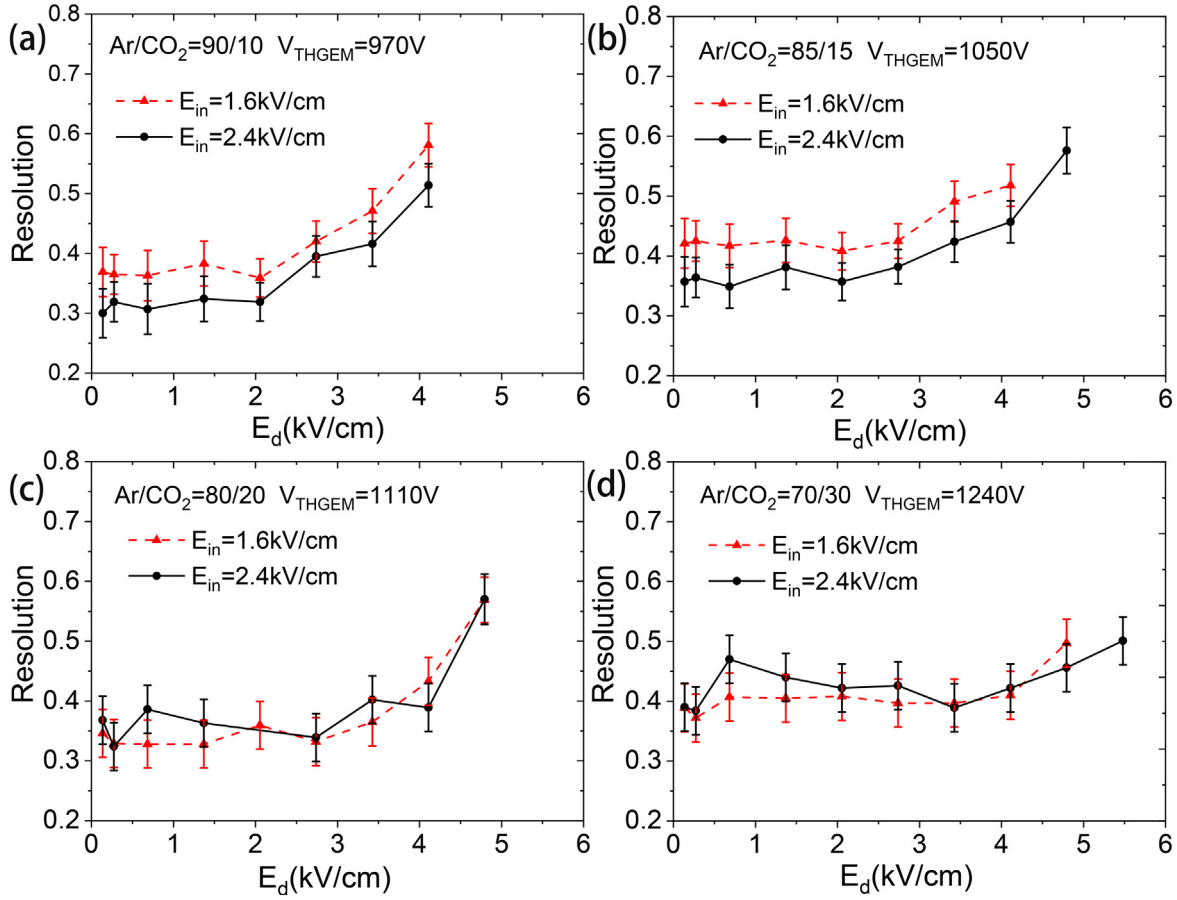

Fig. 8. The resolutions varying with E_d for the THGEM. The error bars represent the standard uncertainties of the data.

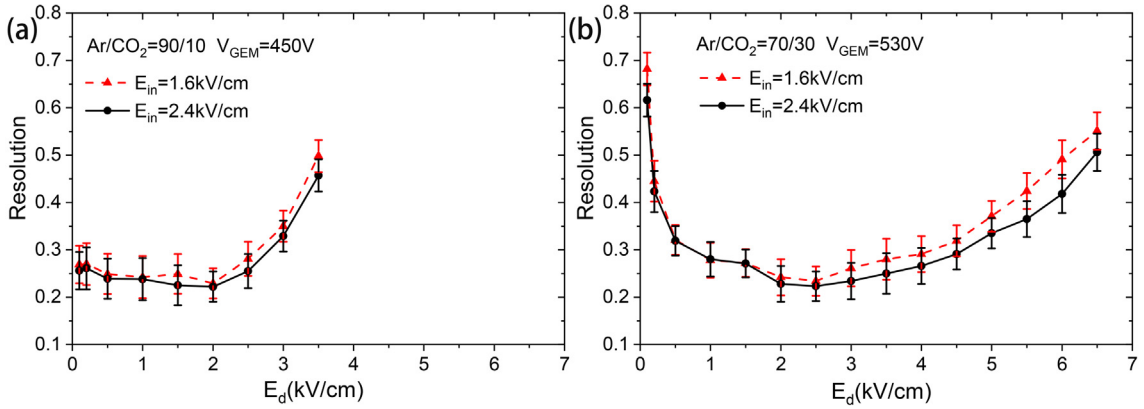

Fig. 9. The resolutions varying with E_d for the standard GEM. The error bars represent the standard uncertainties of the data.

value for the same Ar/CO_2 ratio. The contributions of this component to the resolution are also shown in Figs. 10 and 11.

As shown in Figs. 10 and 11, the variation trend of the calculated resolution with E_d generally matches the experimental results depicted in Fig. 8 for the THGEM, and in Fig. 9 for the standard GEM. However, the absolute values of calculated resolutions are far less than the experimental results. This might be because the contributions from the other factors, e.g., GEM hole size variation, noise, and data acquisition system, are not considered in the calculation [30].

The contributions from the 1st component are about 6.6%, and are independent on the E_d. The 2nd and 3rd components seem to dominate the trend of the resolution variations with E_d. This comparison reveals that there is a big difference between THGEM and standard GEM for Ar/CO_2=90/10 within the uncertainties. For Ar/CO_2=70/30 there is no significant difference. As shown in Fig. 11(b), the 2nd component determines the resolution decrease when E_d is higher than 6 kV/cm for the standard GEM. It can be explained as: increasing E_d can enhance the electric field near hole ends close the drift region [27], so the avalanche enhancement could increase the number of electrons entering holes and

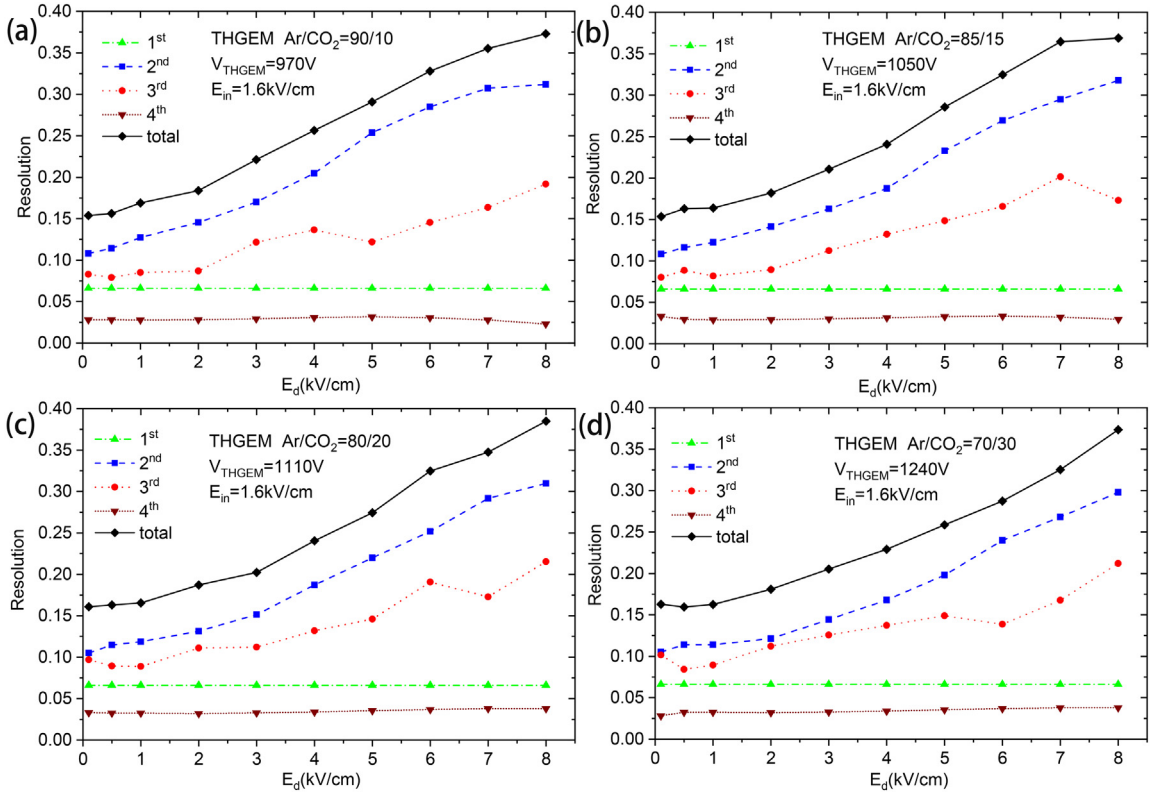

Fig. 10. The simulated energy resolution and its fluctuation contributions from each component in formula (2) for the THGEM working in Ar/CO_2 gas. The 1st, 2nd, 3rd, and 4th contributions represent the fluctuation sources respectively from the primary ionizations, the ECE, the gain above and below the middle plane of the THGEM holes, respectively.

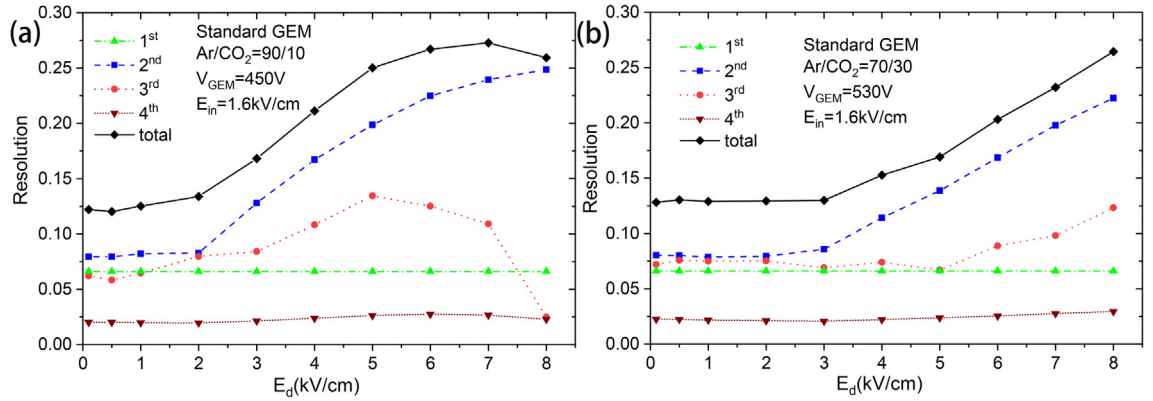

Fig. 11. The simulated energy resolution and its fluctuation contributions from each component in formula (2) for the standard GEM working in Ar/CO_2 gas. The 1st, 2nd, 3rd, and 4th contributions represent the fluctuation sources respectively from the primary ionizations, the ECE, the gain above and below the middle plane of the THGEM holes, respectively.

improves the energy resolution of the standard GEM. The difference of the resolution variations with E_d for the THGEM and standard GEM (in Figs. 10(a) and 11(a)) reveals the different influences of increasing E_d on the variation of ECE (2nd component in formula (2)) and the avalanche near hole ends close to the drift region (which will change the $\overline{N}$ in formula (2)). When E_d is high, increasing E_d decreases ECE and increases its variation, which will deteriorate the energy resolution. Simultaneously, increasing E_d also enhances the electric field near hole ends, and produces more electrons, which will improve the energy resolution. The variation of energy resolution for high E_d results from the competition between the 2nd and 3rd components when increasing E_d.

The last component contributions to energy resolution are less than 3%. It is found that very high E_d can decrease the 4th component, the change of which with E_d can reflect the variation in number of electrons arriving at the middle plane of a GEM.

3.4. *Effective gain variation with* E_{in}

The results of effective gain variation with E_{in} are shown in Fig. 13 for the THGEM. The effective gains increase fast in the low E_{in} range, then a plateau is reached. For Ar/CO_2 = 90/10 and 85/15, the gain increases again above the upper limit of the plateau. These results are consistent with the results found in Ref. [26]. The effective gain has a

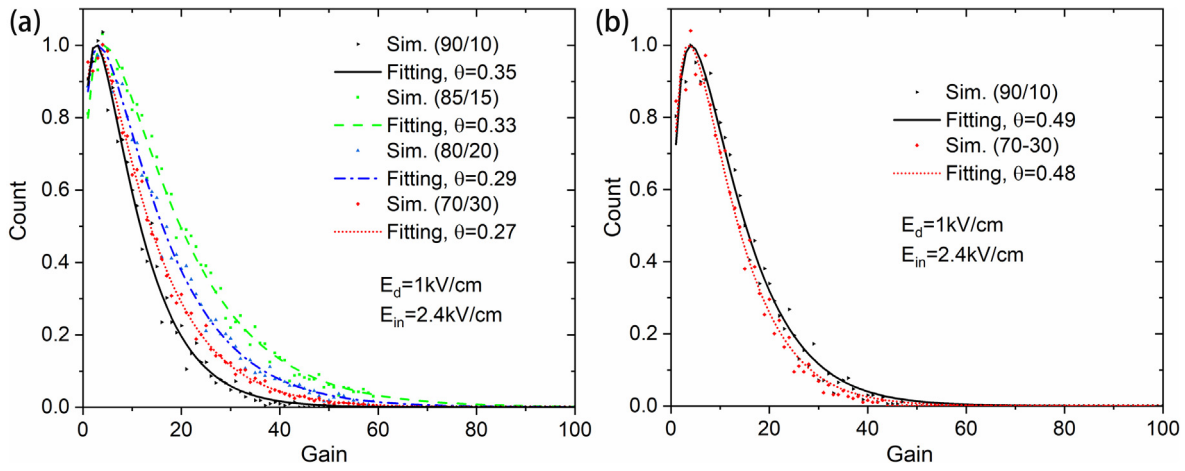

Fig. 12. The simulated gain distribution of single electrons starting from the middle plane of the THGEM and the standard GEM working in Ar/CO_2 gas.

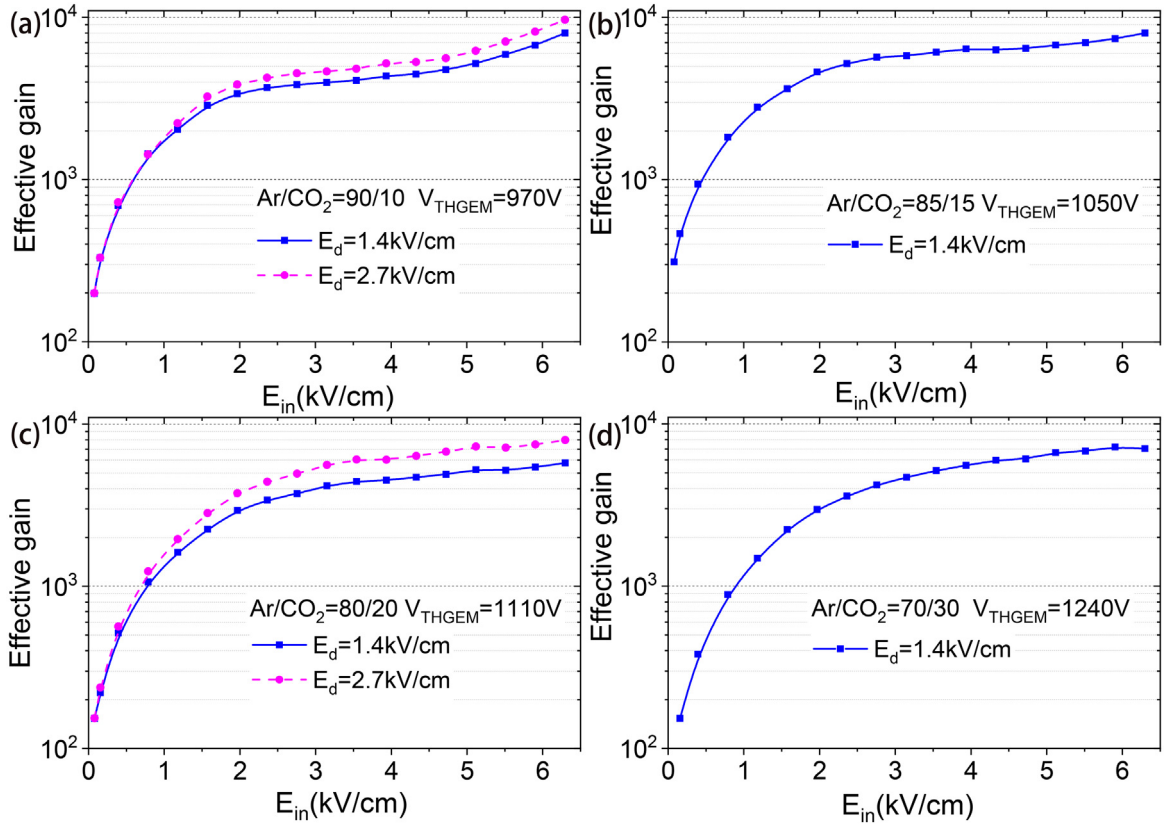

Fig. 13. Effective gain variation with E_{in} for the THGEM.

sharp increase in the low E_{in} range due to the increase of the extraction efficiency of electrons out of the holes. When further increasing E_{in}, a plateau is reached due to the full extraction efficiency. The upper limit of the plateau moves toward higher values when increasing V_{THGEM}. Fig. 14 depicts the measured gain variation with E_{in} for the standard GEM using the same experimental setup, and similar results with the THGEM are found. In Figs. 13(a) and 14(a), effective gains increase again when E_{in} is higher than ~5 kV/cm, and the increase is becoming faster with E_{in}. Similar to the reason for the second increase of gain with E_d, the main contribution of this gain increase might be attributed to the electric field extension out of the holes when E_{in} increases. We will investigate this phenomenon in detail in a future work. Above the plateau, Fig. 15 reveals a faster increase of effective gain with E_{in} for the THGEM than that of the standard GEM, which is attributed to the larger extension of electric fields out of the holes for the THGEM, resulting in a stronger gain enhancement when increasing E_{in}.

3.5. Energy resolution variation with E_{in}

The energy resolution data of the THGEM varying with E_{in} are plotted in Fig. 16. Below ~1 kV/cm, the resolution becomes better with increasing E_{in}. Above ~1 kV/cm, the resolution reaches its lower value and shows slight dependence on E_{in}. In Fig. 17, a similar change of resolution with E_{in} is also found for the standard GEM. In this measurement, the THGEM has the best resolution of about 32%, which is worse than that of the standard GEM (~22%).

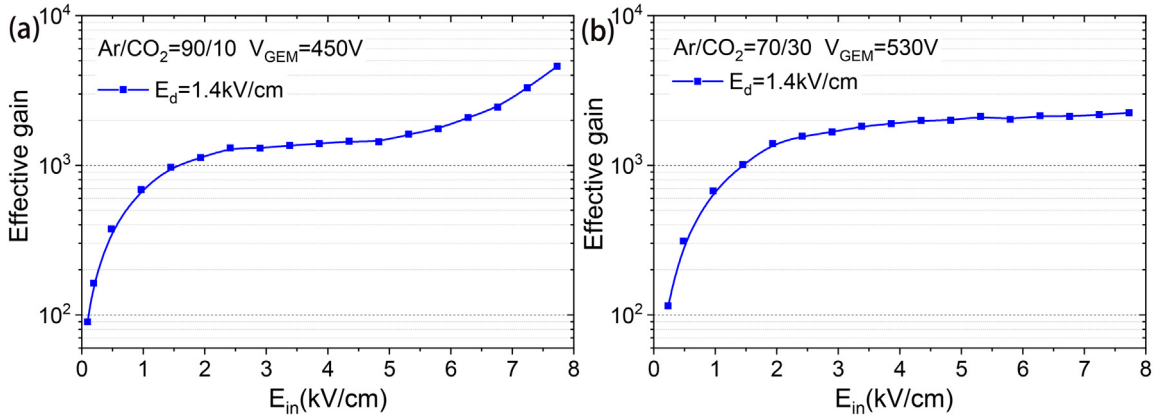

Fig. 14. Effective gain variation with E_{in} for the standard GEM.

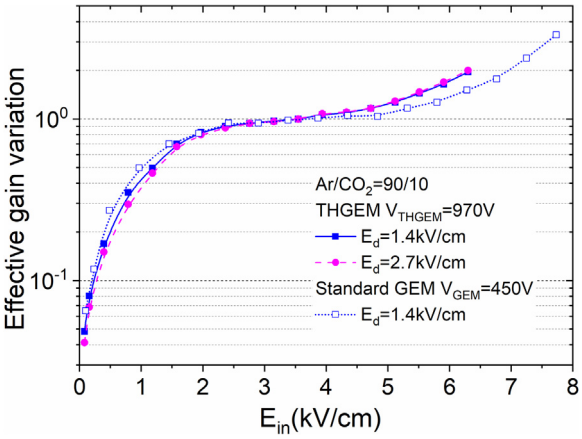

Fig. 15. Effective gain variation with E_{in} for the THGEM and the standard GEM working in Ar/CO_2 (90/10) gas. These data are from Figs. 13(a) and 14(a) and normalized to unity at $E_{in} \approx 3.5$ kV/cm.

3.6. Stability of the THGEM

The long-duration stability performance of the THGEM is shown in Fig. 18. The standard deviation from the averaged value for effective gains, energy resolutions, and count rates during the continuous measurement within 5 h are 0.4%, 1.9%, and 1.1%, respectively. These results confirm the good stability of the THGEM. Data are obtained from the PHS accumulated in 200 s intervals with a threshold of 500 MCA channels.

4. Discussion

The gain and resolution performance of the new THGEM is comprehensively investigated in a wide E_d and E_{in} range with an upper limit of 8 kV/cm. As the gain is a key parameter of GEMs, the possible high gains were selected to carry out the performance investigation in several volume proportions of Ar/CO_2 mixtures. The maximum gain for the THGEM is >2 times higher than for the standard GEM, which confirms the better performance in applications requiring higher gain, e.g., single electron detection. This THGEM has maximum gains lower than the other THGEMs which can have maximum gains larger than 10^4. The lower gain of this THGEM might be ascribed to hole accuracy and the smaller hole size (hole diameter=0.2 mm) compared to the other THGEMs (hole diameter ≥0.4 mm) [10].

The THGEM and standard GEM show different gain variations with E_d in low and high E_d ranges. We interpret the differences using simulations and a simple numerical method to reveal the key factors, by investigating the gain variations with E_d in three E_d stages: the increasing behavior of gain in the low E_d range, the second increase of gain in the high E_d range, and the transition stage between them. The differences are ascribed to the different influence of the E_d change on the ECE and the extension of electric field out of the holes for the THGEM and the standard GEM. A higher E_d makes more electric lines terminate at the top electrode of GEMs and decreases ECE. The THGEM and the standard GEM have different sized holes which determines the extension of electric fields when changing E_d. This extension, which can be reflected by the electric field distribution along the hole axis shown in Figs. 6 and 7, enhances the electric field around hole ends near the drift region and increases the gain of GEMs. In the standard GEMs, the upper limit of the plateau in the low E_d range in the curve of gain variations with E_d can determine the upper limit of the E_d range where the standard GEM has the highest ECE values [27]. For the THGEM, the upper boundary of the first stage (in the low E_d range below the vertical dashed lines in Figs. 4 and 5) is consistent with the upper limit of the E_d range where the ECE values are maximum. Therefore, the measurement of the gain variation with E_d can also be used to investigate ECE for the THGEM, which is essential for determining the suitable E_d value for achieving a higher gain when the THGEM works in cascade mode. This investigation can also explain the continuous increase of gain behavior in the low E_d range for the other THGEMs with rim [10].

The THGEM and standard GEM have the best energy resolutions in the low E_d range, as shown in Figs. 8 and 9. This range matches the low E_d range (below the vertical dashed lines in Figs. 4 and 5) in the gain variation with E_d curves. However, the THGEM has worse resolution than the standard GEM, revealing that THGEM might not be suitable to develop soft X-rays devices for diagnosing plasmas in tokamaks [5]. For the THGEM and standard GEM, the trend of the energy resolution variations with E_d seems to match the simulations well, however the absolute resolution values show large differences between experiment and simulation results. The shape of variation is predominated by the influence on the ECE and the electric field near hole ends close to the drift region when changing E_d. In the very high E_d range in Ar/CO_2 (90/10) gas, the different variations of resolution with E_d between the THGEM and standard GEM can be explained by the different influence of changing E_d on the ECE variations and on the number of electrons entering the holes.

The general gain and resolution variations with E_{in} are similar for the THGEM and standard GEM. The high E_{in} values can help the anode collect the electrons coming from the holes, providing for better energy resolution. At high E_{in}, the gain of the THGEM increases faster than the standard GEM, as the THGEM has larger holes and thus has larger electric field extension out of the holes than the standard GEM.

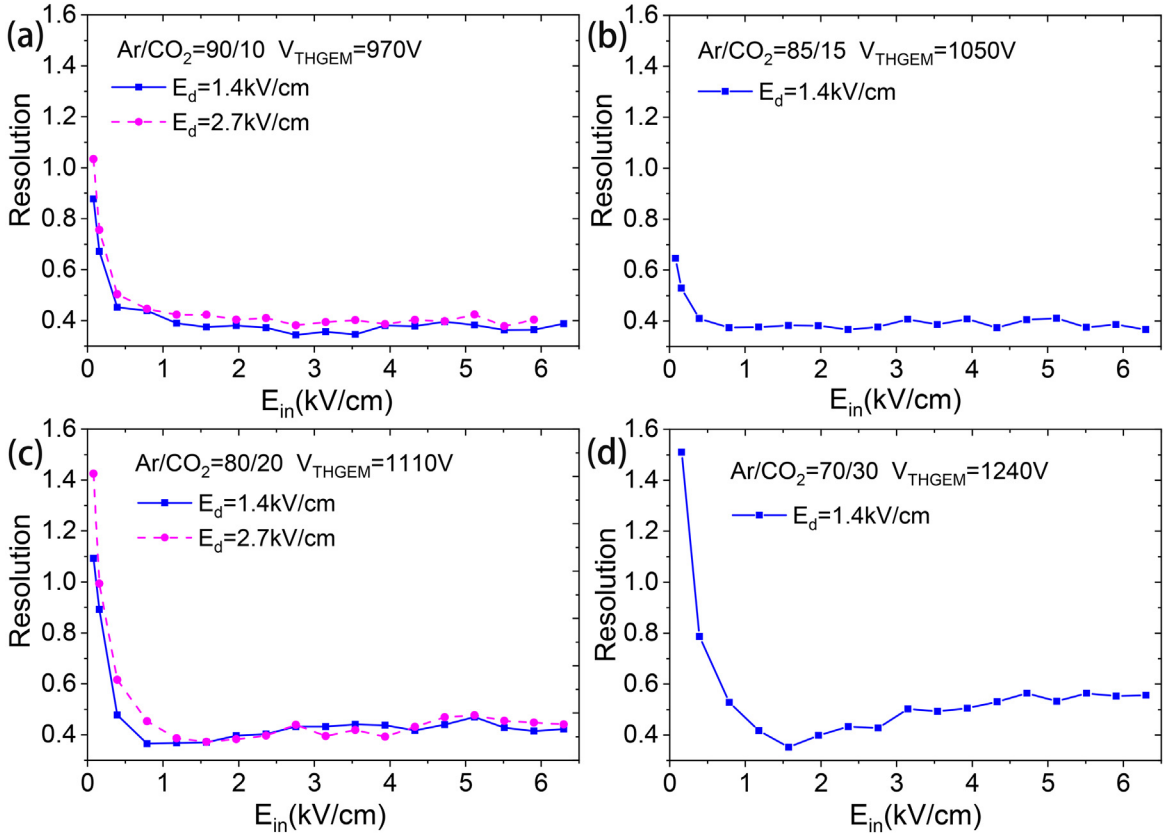

Fig. 16. The resolution varying with E_{in} for the THGEM.

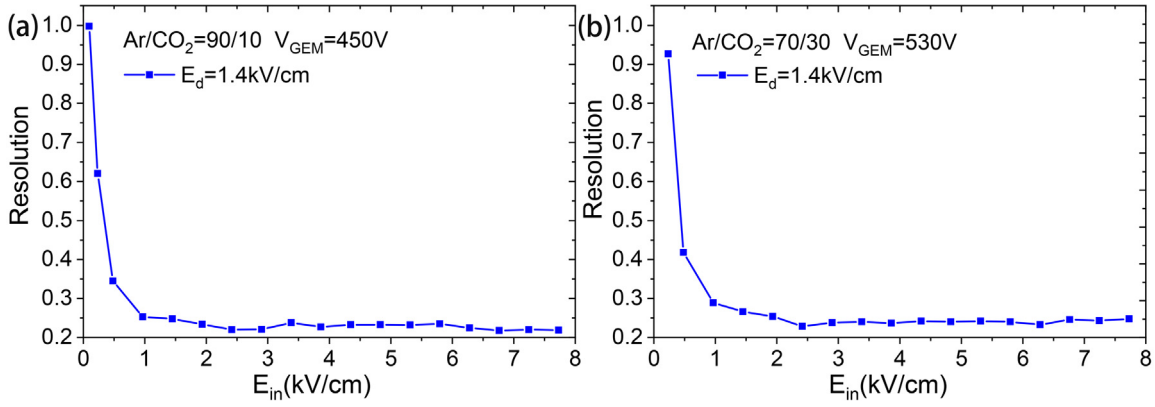

Fig. 17. The resolutions varying with E_{in} for the standard GEM.

5. Conclusion

The systematic investigation on the effective gain and energy resolution using a ^{55}Fe X-ray source reveals some particular operation properties of the THGEM.

The maximum gains for the THGEM are >2 times higher than the standard GEM, indicating the THGEM has great potential in applications requiring higher gain [3,10,28]. There is less dust-free requirement for building a THGEM detector than a standard GEM, and the THGEM detector can work well after being assembled in general working environment.

Simulation and numerical methods are suggested to predict the gain variation with E_d. For the THGEM, the ECE plateau matches the low E_d range in the curves of gain variations with E_d. Therefore, we can determine the suitable E_d for achieving the maximum ECE by investigating the gain variations with E_d, like that done for a standard GEM, even though the gain variations with E_d are very different between the THGEM and the standard GEM.

The THGEM has the best energy resolutions at low E_d and high E_{in} values, similar to the standard GEM. What should be noted is that in high Ar/CO_2 proportions, e.g. 90/10, in high E_d (larger than 6 kV/cm) increasing E_d can improve the energy resolution for the standard GEM, but not for the THGEM. It is ascribed to the competition of the influences of changing E_d on the ECE variations and the number of electrons entering hole.

Higher E_{in} values can help the THGEM anode collect more electrons from holes, therefore achieving higher gains and better energy resolutions. This phenomenon is similar in both the THGEM and the standard

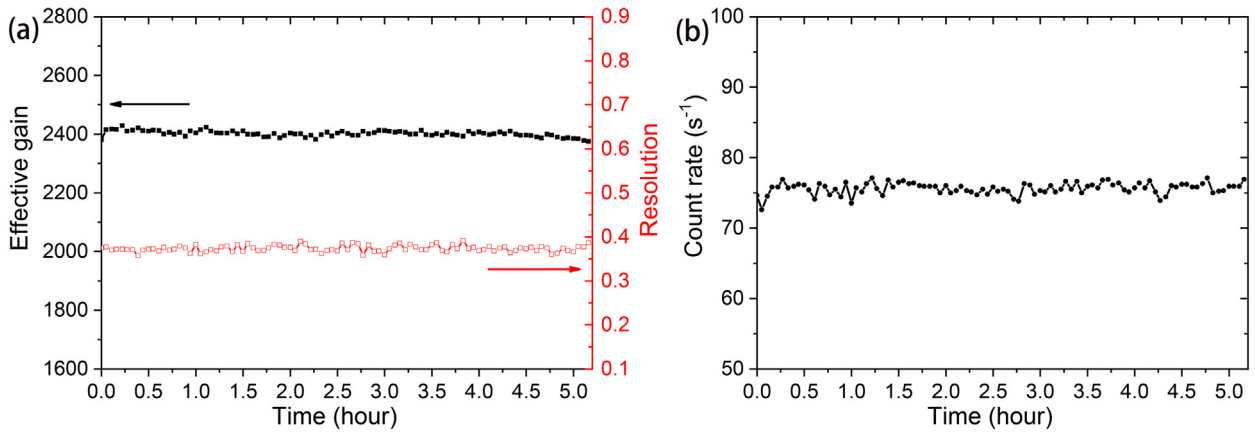

Fig. 18. Time-evolution of effective gain, energy resolution, and count rate of the THGEM at E_d = 1.4 kV/cm, E_{in} = 1.6 kV/cm, and V_{THGEM} = 970 V in Ar/CO_2 (90/10) gas.

GEM. In the high E_{in} range, the THGEM has a faster growth of gain than the standard GEM.

The best energy resolution of the THGEM (32%) is worse than that of the standard GEM (22%). Finally, the relative standard deviation from the averaged value for the effective gain, energy resolution, and count rate is found to be within 1% during 5 h of measurement, demonstrating the good stability of the THGEM.

CRediT authorship contribution statement

Zhimeng Hu: Conceptualization, Methodology, Software, Investigation, Data curation, Visualization. **Andrea Muraro:** Methodology, Software, Investigation, Data curation. **Giuseppe Gorini:** Investigation, Resources, Supervision, Project administration, Funding acquisition. **Oisin McCormack:** Writing - review & editing. **Enrico Perelli Cippo:** Resources. **Marco Tardocchi:** Resources. **Zhijia Sun:** Resources. **Xiaojuan Zhou:** Resources. **Jianrong Zhou:** Resources. **Yuguang Xie:** Resources. **Yuanbo Chen:** Resources. **Hui Zhang:** Resources. **Tieshuan Fan:** Resources. **Gabriele Croci:** Methodology, Software, Investigation, Data curation, Resources, Supervision.

Declaration of competing interest

The authors declare that they have no known competing financial interests or personal relationships that could have appeared to influence the work reported in this paper.

Acknowledgments

This work was supported within the Research Grant agreement No. 19A2/11 in research activities at the University of Milano – Bicocca. We also received finical support from the National Key R&D Program of China (No. 2017YFA0403702), the National Natural Science Foundation of China (No. 11635012), and Youth Innovation Promotion Association CAS, China.

References

[1] F. Sauli, From bubble chambers to electronic systems: 25 years of evolution in particle detectors at CERN (1979–2004), Phys. Rep. 403–404 (2004) 471–504.

[2] G. Croci, et al., Characterization of a thermal neutron beam monitor based on gas electron multiplier technology, Prog. Theor. Exp. Phys. 2014 (2014) 83H01;
G. Croci, et al., Gem-based thermal neutron beam monitors for spallation sources, Nucl. Instrum. Methods Phys. Res. A 732 (2013) 217-220.

[3] F. Sauli, The gas electron multiplier (GEM): Operating principles and applications, Nucl. Instrum. Methods Phys. Res. A 805 (2016) 2–24.

[4] J. Giovinazzo, et al., First direct observation of two protons in the decay of ^{45}fe *with a time-projection chamber*, Phys. Rev. Lett. 99 (2007) 102501.

[5] E. Li, et al., First results of the 2D gas electron multiplier in the dominant electron heating scenario on EAST, Nucl. Fusion 59 (2019) 106030;
A. Muraro, et al., Development and characterization of a new soft x-ray diagnostic concept for tokamaks, J. Instrum. 14 (2019) C08012.

[6] S. Agosteo, Overview of novel techniques for radiation protection and dosimetry, Radiat. Meas. 45 (2010) 1171–1177.

[7] G. Croci, et al., Measurements of γ-ray sensitivity of a GEM based detector using a coincidence technique, J. Instrum. 8 (2013) P04006.

[8] F. Sauli, GEM: A new concept for electron amplification in gas detectors, Nucl. Instrum. Methods Phys. Res. A 386 (1997) 531–534.

[9] R.C. Roque, et al., Spatial resolution properties of krypton-based mixtures using a 100μm thick gas electron multiplier, J. Instrum. 13 (2018) P10010.

[10] M. Alexeev, et al., The gain in thick GEM multipliers and its time-evolution, J. Instrum. 10 (2015) P03026.

[11] A. Breskin, et al., The THGEM: A thick robust gaseous electron multiplier for radiation detectors, Nucl. Instrum. Methods Phys. Res. A 623 (2010) 132–134.

[12] S. Dalla Torre, Gaseous counters with CsI photocathodes: The COMPASS RICH, Nucl. Instrum. Methods Phys. Res. A 970 (2020) 163768;
M. Alexeev, et al., The quest for a third generation of gaseous photon detectors for cherenkov imaging counters, Nucl. Instrum. Methods Phys. Res. A 610 (2009) 174-177;
M. Alexeev, et al., Thgem based photon detector for cherenkov imaging applications, Nucl. Instrum. Methods Phys. Res. A 617 (2010) 396-397;
M. Alexeev, et al., Micropattern gaseous photon detectors for cherenkov imaging counters, Nucl. Instrum. Methods Phys. Res. A 623 (2010) 129-131.

[13] J. Agarwala, et al., The MPGD-based photon detectors for the upgrade of COMPASS RICH-1 and beyond, Nucl. Instrum. Methods Phys. Res. A 936 (2019) 416–419.

[14] M. Alexeev, et al., Ion backflow in thick GEM-based detectors of single photons, J. Instrum. 8 (2013) P01021.

[15] S. Bressler, Beam studies of novel THGEM-based potential sampling elements for digital hadron calorimetry, J. Instrum. 8 (2013) P07017.

[16] S. Dalla Torre, et al., R & D Proposal RD51 Extension beyond 2018, Report NO.: CERN-LHCC-2018-016/ LHCC-SR-006, CERN, Geneva, Switzerland, 2018.

[17] A. Bondar, et al., On the low-temperature performances of THGEM and THGEM/G-APD multipliers in gaseous and two-phase Xe, J. Instrum. 6 (2011) P07008.

[18] G. Albani, et al., High-rate measurements of the novel BAND-GEM technology for thermal neutron detection at spallation sources, Nucl. Instrum. Methods Phys. Res. A 957 (2020) 163389;
E. Perelli Cippo, et al., A GEM-based thermal neutron detector for high counting rate applications, J. Instrum. 10 (2015) P10003.

[19] J. Zhou, et al., A novel ceramic GEM used for neutron detection, Nucl. Eng. Technol. 52 (2020) 1277–1281.

[20] G. Croci, et al., A high-efficiency thermal neutron detector based on thin 3D$^{10}B_4c$ *converters for high-rate applications*, Europhys. Lett. 123 (2018) 52001;
A. Muraro, G. Croci, Review of MPGD applications for neutron detection, J. Instrum. 14 (2019) C04005.

[21] G. Croci, et al., Diffraction measurements with a boron-based GEM neutron detector, Europhys. Lett. 107 (2014) 12001;
G. Croci, et al., I-BAND-GEM: A new way for improving BAND-GEM efficiency to thermal and cold neutrons, Eur. Phys. J. Plus 134 (2019) 166;
G. Croci, et al., The CNESM neutron imaging diagnostic for SPIDER beam source, Fusion Eng. Des. 146 (2019) 660.

[22] S. Khezripour, et al., A new approach for alpha radiography by triple THGEM using Monte Carlo simulation and measurement, J. Instrum. 13 (2018) P05024.

[23] Z. Anjomani, et al., Development of a multi-element microdosimetric detector based on a thick gas electron multiplier, Nucl. Instrum. Methods Phys. Res. A 847 (2017) 117–124.

[24] A.V. Klyachko, et al., A GEM-based dose imaging detector with optical readout for proton radiotherapy, Nucl. Instrum. Methods Phys. Res. A 694 (2012) 271–279.
[25] See www.bronkhorst.com for product: EL-FLOW SELECT F-201CV.
[26] S. Bachmann, et al., Charge amplification and transfer processes in the gas electron multiplier, Nucl. Instrum. Methods Phys. Res. A 438 (1999) 376–408.
[27] Z.M. Hu, et al., Interpretation of effective gain variations with the drift electric field for a ceramic thick gas electron multiplier, Nucl. Instrum. Methods Phys. Res. A 988 (2021) 164907.
[28] H.B. Liu, et al., The performance of thinner-THGEM, Nucl. Instrum. Methods Phys. Res. A 659 (2011) 237–241.
[29] U. Fano, On the theory of ionization yield of radiations in different substances, Phys. Rev. 70 (1946) 44.
[30] E. Ruiz-Choliz, et al., Modelling the behaviour of microbulk micromegas in xenon/trimethylamine gas, Nucl. Instrum. Methods Phys. Res. A 799 (2015) 137–146.